nature sustainability

Article

https://doi.org/10.1038/s41893-023-01237-y

Electrolyte design for lithium-ion batteries with a cobalt-free cathode and silicon oxide anode

In the format provided by the authors and unedited

Table of Contents

Supplementary Note 1

Note that the potentials of all Li^+-related reactions (e.g., Li, SiO_x, and $Li_4Ti_5O_{12}$ anodes, and $LiFePO_4$ and $LiNi_{0.5}Mn_{1.5}O_4$ cathodes) depend on the change in the Gibbs free energy of Li^+ in the electrolyte, and hence the shifts occur simultaneously in identical magnitudes. Therefore, the voltage of a two-electrode cell does not change even with a significant potential shift in both the anode and cathode (Supplementary Fig. SN1). The potential shift of each electrode cannot be observed without using a standard electrode such as ferrocene (Fc/Fc^+), of which potential remains independent of the electrolyte.

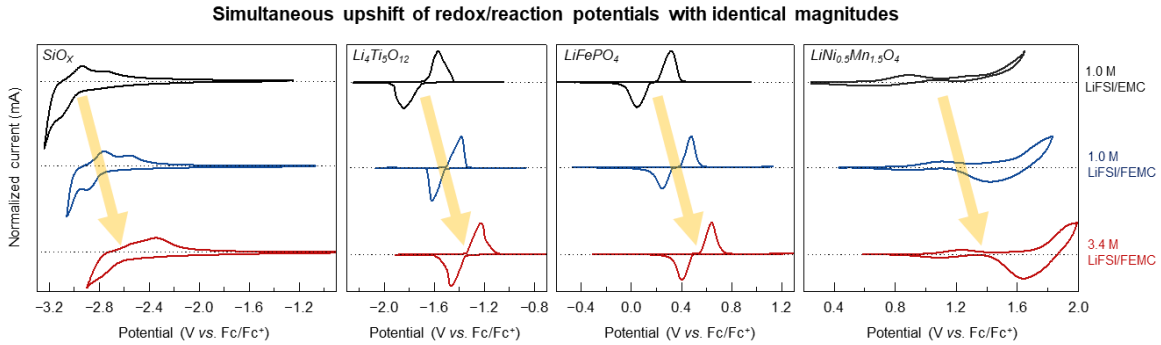

Supplementary Figure SN1. Cyclic voltammograms representing the simultaneous and identical-magnitude potential shift (yellow arrows) of electrodes and the unchanged battery voltage. The reaction potentials of each electrode were measured using ferrocene (Fc/Fc^+), which is an IUPAC-recommended internal standard providing electrolyte-independent redox potential.

Supplementary Table 1. Basic physicochemical properties of the prepared electrolytes at 25 °C.

	Concentration (mol kg^{-1})	Density (g cm^{-3})	Viscosity (mPa s)	Ionic conductivity (mS cm^{-1})
1.0 M LiFSI/EMC	1.1	1.1	1.9	6.6
1.0 M LiFSI/FEMC	0.8	1.4	3.3	1.8
3.4 M LiFSI/FEMC	3.4	1.6	69	1.2

Supplementary Table 2. Cell lengths and numbers of solvent molecules/ions used in the molecular dynamics (MD) simulations.

	Cell length (Å)	N (EMC or FEMC)	N (Li^+)	N (FSI^-)
1.0 M LiFSI/EMC	52.18	792	90	90
1.0 M LiFSI/FEMC	54.50	780	100	100
3.4 M LiFSI/FEMC	52.30	540	300	300

Supplementary Table 3. Comparison data regarding SiO_x-based full cells. The cathode loading levels marked with asterisks are estimated based on the anode masses and capacities and negative/positive (N/P) ratios. [1–20] The data obtained from this study is highlighted in red.

Cathode	Cathode loading level (mg/cm^2)	Anode	Anode capacity (mAh/g)	Electrolyte	Electrolyte amount (µl)	Separator	N/P ratio	Upper cut-off voltage (V)	Charge / Discharge rate	Capacity retention	Cell type	Remarks	Reference
$LiNi_{0.5}Co_{0.2}Mn_{0.3}O_2$	-	SiO/C	749	1 M $LiPF_6$/EC:DEC (1:1) + 5 wt% FEC	-	Celgard 2400	cathode excess	4.3	0.5 C / 0.5 C	94 % @ 160 cyc	2032 coin	Pre-lithiated anode (Fully lithiated anode)	1
$LiNi_{0.8}Co_{0.15}Al_{0.05}O_2$	14	SiO/C	978	1 M $LiPF_6$/EC:DEC (1:1) + 5 wt% FEC	200	Celgard 2400	1.1	4.2	1.0 C / 1.0 C	61 % @ 100 cyc	2032 coin	Pre-lithiated anode	2
$LiNi_{0.5}Co_{0.2}Mn_{0.3}O_2$	11.5	SiO_x/PPy	1280	1 M $LiPF_6$/EC:DEC (1:1) + 30 wt% FEC	60	Celgard 2400	-	4.3	1.0 C / 1.0 C	76 % @ 90 cyc	2325 coin	Pre-lithiated anode	3
$LiNi_{0.6}Co_{0.2}Mn_{0.2}O_2$	-	SiO_x	743	-	-	-	1.05	4.3	0.5 C / 0.5 C	74 % @ 200 cyc	coin	Pre-lithiated anode	4
$LiCoO_2$	5.5 ~ 8.0 *	SiO_x	1145	1 M $LiPF_6$/EC:DEC (1:1) + 3 wt% VC	-	-	1.1	4.3	1.0 C / 1.0 C	90 % @ 50 cyc	2032 coin	Pre-lithiated anode	5
$LiNi_{0.6}Co_{0.2}Mn_{0.2}O_2$	20	SiO	1070	Gel polymer electrolyte + 1 M $LiPF_6$/EC:DEC (1:1) + 10wt% FEC	-	Polymer membrane	1.18	4.2	0.33 C / 0.33 C	70 % @ 350 cyc	2016 coin	Pre-activated anode (Almost delithiated anode)	6
$LiFePO_4$	6 ~ 12	$SiO_{1.09}$/C	999	1 M $LiPF_6$/EC:DMC (1:1)	-	-	cathode:anode 4:1 (w:w)	3.8	0.2 C / 0.2 C	88 % @ 100 cyc	2016 coin	Pre-lithiated anode	7
$LiNi_{0.33}Co_{0.33}Mn_{0.33}O_2$	-	SiO	1150	1 M $LiPF_6$/EC:DEC (3:7) + 30 wt% FEC	-	Celgard 2400	-	4.2	0.3 C / 0.3 C	87 % @ 100 cyc	2325 coin	With stabilized lithium metal powder	8
$LiCoO_2$	~ 4.0 *	Si/SiO_2	1782	1 M $LiPF_6$/EC:DMC:FEC (1:1:0.1)	-	Celgard 2300	1.2	4.0	1.0 C / 1.0 C	60 % @ 100 cyc	2016 coin	-	9
$LiNi_{0.6}Co_{0.1}Mn_{0.1}O_2$	6 ~ 8	Si/SiO_2/C/Graphite	972	1 M $LiPF_6$/EC:DEC (1:1) + 10 vol% FEC	80	Celgard 2400	1.2	4.2	1.0 C / 1.0 C	61 % @ 100 cyc	Three-electrode Swagelok	-	10
$LiNi_{0.6}Co_{0.2}Mn_{0.2}O_2$	18.5	SiO_x/Graphite	655	1 M $LiPF_6$/EC:DEC:DMC (1:1:1) + 5 vol % FEC	-	Celgard 2500	1.1	4.2	0.2C / 0.2 C	93 % @ 100 cyc	pouch cell	Pre-lithiated anode	11
$LiNi_{0.8}Co_{0.15}Al_{0.05}O_2$	19.4 or 27.8	Polymer funtionalized SiO_x/C	~1000	1 M $LiPF_6$/EC:DEC (1:1) + 7.5 wt% FEC + 0.5 wt% VC	100	PE	1.1	4.2	0.5 C / 0.5 C	82.5 % @ 150 cyc (cathode 19.4 mg/cm^2) 78 % @ 50cyc (cathode 27.8 mg/cm^2)	2032 coin	-	12
$LiFePO_4$	4.0 ~ 5.5 *	N-doped SiO_x/C	797	1.3 M $LiPF_6$/EC:DEC:FEC (30:60:10)	-	-	1.2	3.8	2.0 C / 2.0 C	89% @ 350 cyc	2032 coin	Pre-lithiated anode	13
$LiNi_{0.6}Co_{0.2}Mn_{0.2}O_2$	2.4 ~ 3.6	N-doped SiO_x/C	970	1 M $LiPF_6$ EC/DMC	-	-	cathode:anode 3:1 (w:w)	4.3	100 mA/g (~0.5 C) /100 mA/g (~0.5 C)	88.5% @ 150 cyc	2032 coin	Pre-lithiated anode	14
$LiFePO_4$	6 ~ 9	Si/SiO_2/C	~1000	1 M $LiPF_6$/EC:DMC (1:1) + 10 vol% FEC	-	-	cathode:anode 6:1 (w:w)	3.8	0.2 C / 0.2 C	92 % @ 100 cyc	2016 coin	Pre-activated anode	15
$LiNi_{0.6}Co_{0.2}Mn_{0.2}O_2$ $LiFePO_4$	7.2 6.0	SiO/C	1456 ~ 1580	1 M $LiPF_6$/EC:DEC (1:1) + 10 vol% FEC	100	Cellulose	1.2 1.4	4.2 4.2	0.1 C / 0.1 C 0.2 C / 0.2 C	49 % @ 40 cyc 52 % @ 100 cyc	2016 coin	Pre-lithiated anode	16
$LiNi_{0.6}Co_{0.2}Mn_{0.2}O_2$	7.1	N-doped SiO_x/C	700	1 M $LiPF_6$/EC:DEC (1:1) + 10 % FEC	100	Cellulose	1.2	-	0.1 C / 0.1 C	46 % @ 50 cyc	2016 coin	Pre-lithiated anode	17
$LiNi_{0.5}Co_{0.2}Mn_{0.3}O_2$	-	Exfoliated N-doped carbon nanosilices supported SiOx	1252	1 M $LiPF_6$/EC:EMC:DMC (1:1:1) + 7 % FEC	-	Celgard 2400	1.1	4.3	1.5 C / 1.5 C	62 % @ 100 cyc	2025 coin	Pre-activated anode	18
$LiFePO_4$	-	Si/C	1568	1 M $LiPF_6$/EC:DEC:FEC (3:7:1)	-	Celgard 2500	1.15	3.8	0.5 C / 0.5 C	93.5 % @ 100 cyc	2032 coin	Pre-lithiated anode	19
$LiNi_{0.6}Co_{0.1}Mn_{0.1}O_2$	8.6 ~ 9.8	SiO_x	1518	1 M $LiPF_6$/EC:EMC (1:2) + 0.01 M LiFSI + 2 % $LiPO_2F_2$	-	-	cathode:anode 4.5:1 (w:w)	4.3	1.0 C / 1.0 C	94.8 % @ 100 cyc	2032 coin	-	20
$LiNi_{0.8}Mn_{1.2}O_4$:AB :LiPAA (85:10:5)	3	SiO_x/C:AB:PAI (70:15:15)	1615	3.4 M LiFSI/FEMC	80	Glass fiber (190µm thickness)	1.8	4.9	0.2 C / 0.2 C	85 % @ 300 cyc	2032 coin	Pre-activated anode 4.9 - 3.5 V	This work
	5				80		1.5		0.5 C / 0.5 C	96 % @ 500 cyc			
	12			3.4 M LiFSI/FEMC	40		1.2		0.3 C / 1.0 C	72 % @ 500 cyc			
	11			3.4 M LiFSI/FEMC + 10 wt% FEC			1.1			75 % @ 500 cyc			
	12			3.4 M LiFSI/FEMC + 1 wt% $LiPO_2F_2$			1.0			83 % @ 500 cyc			
	20			3.4 M LiFSI/FEMC + 10 wt% FEC + 1 wt% $LiPO_2F_2$			1.1			85 % @ 500 cyc			
$LiNi_{0.8}Mn_{1.2}O_4$:Blended carbons :LiPAA (80:15:5)	20						1.2			89 % @ 500 cyc / 73 % @ 1000 cyc		Pre-activated anode 4.9 - 3.0 V (Reproducibility test)	
	21						1.2			90 % @ 500 cyc / 74 % @ 1000 cyc			
	19						1.3			95 % @ 500 cyc / 79 % @ 1000 cyc			
	19						1.3			92 % @ 500 cyc / 77 % @ 1000 cyc			

Supplementary Note 2

AC and UCV represent the anode capacity and upper cut-off voltage of the full cell, respectively. As the values of AC and UCV increase, an electrolyte with a higher redox stability is required for stable full-cell operation.[21] The cycling stability is represented by the lifetime (cycle number) of the full cell at a certain C-rate.[21–23] To compare the lifetimes, the cycle number is normalized to a value based on a C-rate of 0.5C.[22,23] The capacity retention is normalized to a value based on the normalized cycle number as a reference.[22–25]

$$\textit{Normalized cycle number (NCN)} = cycle\ number \times \frac{0.5\ C-rate}{cycled\ C-rate}$$

$$\textit{Normalized capacity retention per cycle (NCR)} = 100 \times 10^{\frac{log_{10}(Capacity\ retention/100)}{Normalized\ cycle\ number}}$$

Notably, the cycle stabilities of full cells should be carefully compared based on the electrode loading level, N/P ratio, upper cut-off voltage, electrolyte amount, cell type, etc. To the best of our knowledge, this is the first report of stable $SiO_x|LiNi_{0.5}Mn_{1.5}O_4$ batteries with upper cut-off voltages of 4.9 V under practical conditions (high cathode loading level: ~21 mg cm^{-2}, limited amount of electrolyte: 40 μL, and slow C-rates of $0.3C_{charge}$ and $1.0C_{discharge}$).

Supplementary Table 4. Normalized data from Table S3, as shown in Fig. 6b. The data obtained from this study is highlighted in red.

Cathode	Anode	Anode capacity (mAh/g) (x-axis)	Upper cut-off voltage (V) (y-axis)	Charge / Discharge rate	Capacity retention	NCN (-) (color)	NCR (%) (diameter)	Reference
$LiNi_{0.5}Co_{0.2}Mn_{0.3}O_2$	SiO_x/C	749	4.3	0.5 C / 0.5 C	94 % @ 160 cyc	160	99.96	1
$LiNi_{0.8}Co_{0.15}Al_{0.05}O_2$	SiO_x/C	978	4.2	1.0 C / 1.0 C	61 % @ 100 cyc	50	99.02	2
$LiNi_{0.5}Co_{0.2}Mn_{0.3}O_2$	SiO_x/PPy	1280	4.3	1.0 C / 1.0 C	76 % @ 90 cyc	45	99.39	3
$LiNi_{0.6}Co_{0.2}Mn_{0.2}O_2$	SiO_x	743	4.3	0.5 C / 0.5 C	74 % @ 200 cyc	200	99.87	4
$LiCoO_2$	SiO_x	1145	4.3	1.0 C / 1.0 C	90 % @ 50 cyc	25	99.58	5
$LiNi_{0.5}Co_{0.2}Mn_{0.3}O_2$	SiO	1070	4.2	0.33 C / 0.33 C	70 % @ 350 cyc	583	99.94	6
$LiFePO_4$	$SiO_{1.63}$/C	999	3.8	0.2 C / 0.2 C	88 % @ 100 cyc	250	99.95	7
$LiNi_{0.33}Co_{0.33}Mn_{0.33}O_2$	SiO	1150	4.2	0.3 C / 0.3 C	87 % @ 100 cyc	167	99.92	8
$LiCoO_2$	Si/SiO_2	1782	4.0	1.0 C / 1.0 C	60 % @ 100 cyc	50	98.98	9
$LiNi_{0.8}Co_{0.1}Mn_{0.1}O_2$	Si/SiO_2/C/Graphite	972	4.2	1.0 C / 1.0 C	61 % @ 100 cyc	50	99.02	10
$LiNi_{0.8}Co_{0.1}Mn_{0.1}O_2$	SiO_x/Graphite	655	4.2	0.2C / 0.2 C	93 % @ 100 cyc	250	99.97	11
$LiNi_{0.8}Co_{0.15}Al_{0.05}O_2$	Polymer funtionalized SiO_x/C	~1000	4.2	0.5 C / 0.5 C	82.5 % @ 150 cyc 78 % @ 50cyc	150	99.87	12
$LiFePO_4$	N-doped SiO_x/C	797	3.8	2.0 C / 2.0 C	89 % @ 350 cyc	88	99.87	13
$LiNi_{0.6}Co_{0.2}Mn_{0.2}O_2$	N-doped SiO_x/C	970	4.3	100 mA/g (~0.5 C) /100 mA/g (~0.5 C)	88.5% @ 150 cyc	150	99.92	14
$LiFePO_4$	Si/SiO_2/C	~1000	3.8	0.2 C / 0.2 C	92 % @ 100 cyc	250	99.97	15
$LiNi_{0.6}Co_{0.2}Mn_{0.2}O_2$ $LiFePO_4$	SiO/C	1456 ~ 1580	4.2 4.2	0.1 C / 0.1 C 0.2 C / 0.2 C	49 % @ 40 cyc 52 % @ 100 cyc	200 250	99.64 99.74	16
$LiNi_{0.6}Co_{0.2}Mn_{0.2}O_2$	N-doped SiO_x/C	700	-	0.1 C / 0.1 C	46 % @ 50 cyc	250	99.69	17
$LiNi_{0.3}Co_{0.3}Mn_{0.3}O_2$	Exfoliated N-doped carbon nanoslices supported SiOx	1252	4.3	1.5 C / 1.5 C	62 % @ 100 cyc	33	98.60	18
$LiFePO_4$	SiO_x/C	1568	3.8	0.5 C / 0.5 C	93.5 % @ 100 cyc	100	99.93	19
$LiNi_{0.8}Co_{0.1}Mn_{0.1}O_2$	SiO_x	1518	4.3	1.0 C / 1.0 C	94.8 % @ 100 cyc	50	99.89	20
$LiNi_{0.5}Mn_{1.5}O_4$	**SiO_x/C**	**1615**	**4.9**	**0.2 C / 0.2 C**	**85 % @ 300 cyc**	**750 (Figure 6b)**	**99.98 (Figure 6b)**	**This work**
				0.5 C / 0.5 C	**96 % @ 500 cyc**	**500**	**99.99**	
				0.3 C / 1.0 C	**72 % @ 500 cyc**	**385**	**99.92**	
					75 % @ 500 cyc	**385**	**99.93**	
					83 % @ 500 cyc	**385**	**99.95**	
					85 % @ 500 cyc	**385**	**99.96**	
					89 % @ 500 cyc / 73 % @ 1000 cyc	**385 / 770**	**99.97 / 99.96**	
					90 % @ 500 cyc / 74 % @ 1000 cyc	**385 / 770**	**99.97 / 99.96**	
					95 % @ 500 cyc / 79 % @ 1000 cyc	**385 / 770**	**99.99 / 99.97**	
					92 % @ 500 cyc / 77 % @ 1000 cyc	**385 / 770**	**99.98 / 99.97**	

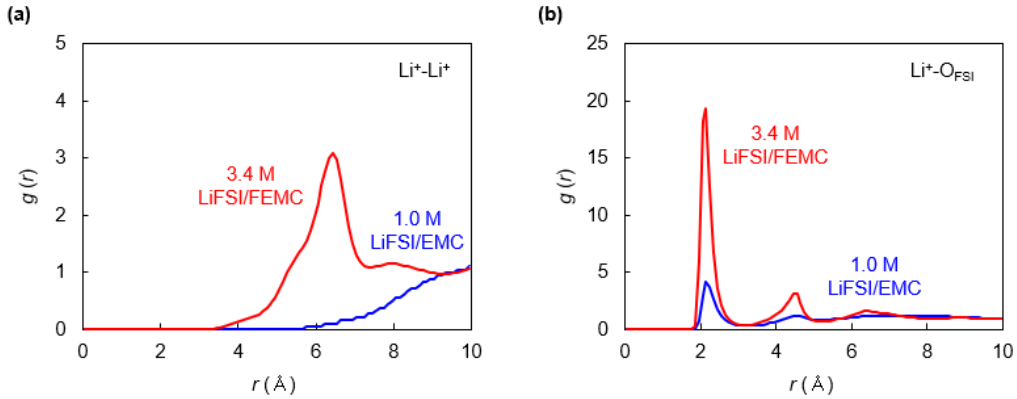

Supplementary Figure 1. Radial distribution functions of 1.0 M $LiN(SO_2F)_2$ (LiFSI)/ethyl methyl carbonate (EMC) and 3.4 M LiFSI/methyl (2,2,2-trifluoroethyl) carbonate (FEMC), as calculated via MD simulations.

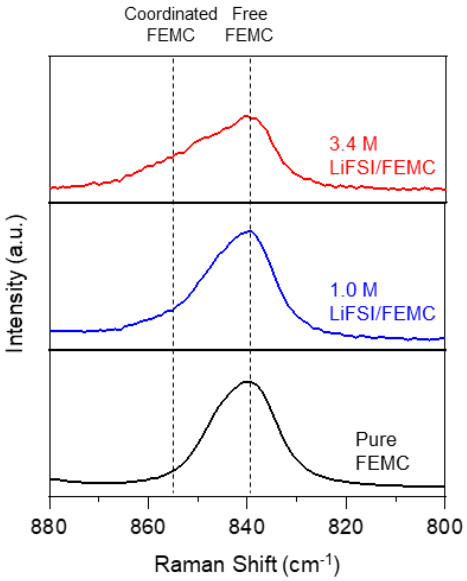

Supplementary Figure 2. Characterization of the solution structures of the LiFSI/FEMC electrolytes via Raman spectroscopy. FEMC exhibits a weak solvating power, which promotes ion-pair formation.

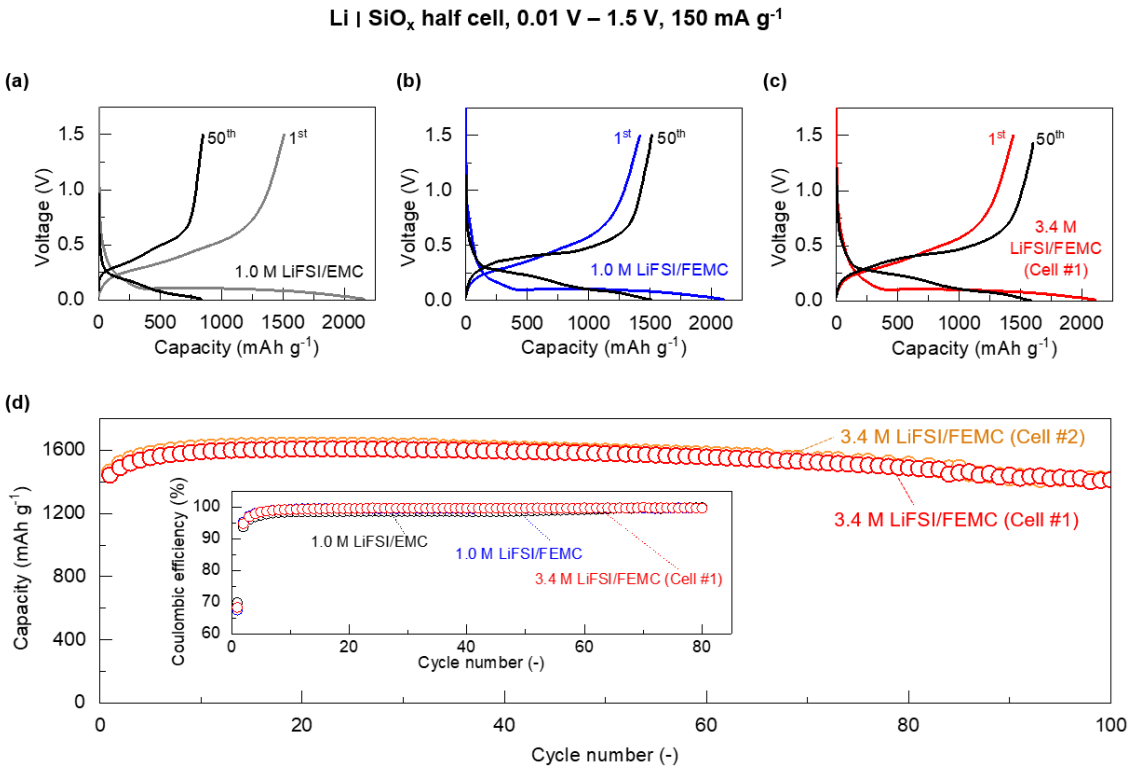

Supplementary Figure 3. (a–c) Charge and discharge curves and (d) reproducibility of Li|SiO_x half-cells with 3.4 M LiFSI/FEMC. The inset in (d) shows the Coulombic efficiencies of the cells with the given electrolytes. The loading levels of the SiO_x electrodes were 1 mg cm^{-2}. Combined separators, composed of polypropylene (PP) and glass fiber separators, were used.

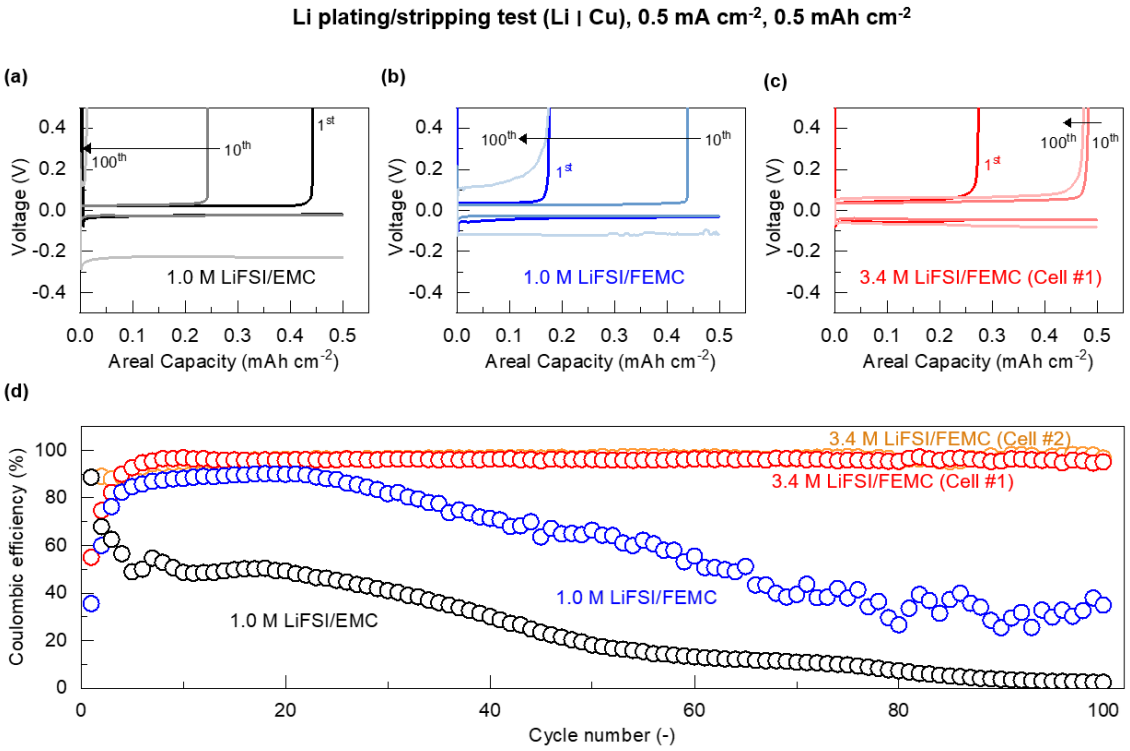

Supplementary Figure 4. Voltage curves of Li|Cu cells with (a) 1.0 M LiFSI/EMC, (b) 1.0 M LiFSI/FEMC, and (c) 3.4 M LiFSI/FEMC electrolytes. (d) Coulombic efficiencies during Li plating/stripping reactions on Cu foils in the given electrolytes. Cells #1 and #2 represent the cell-to-cell reproducibility of cells with 3.4 M LiFSI/FEMC. The Coulombic efficiency of Li plating/stripping is drastically improved in 3.4 M LiFSI/FEMC. A combined separator, composed of PP and glass fiber separators, was used.

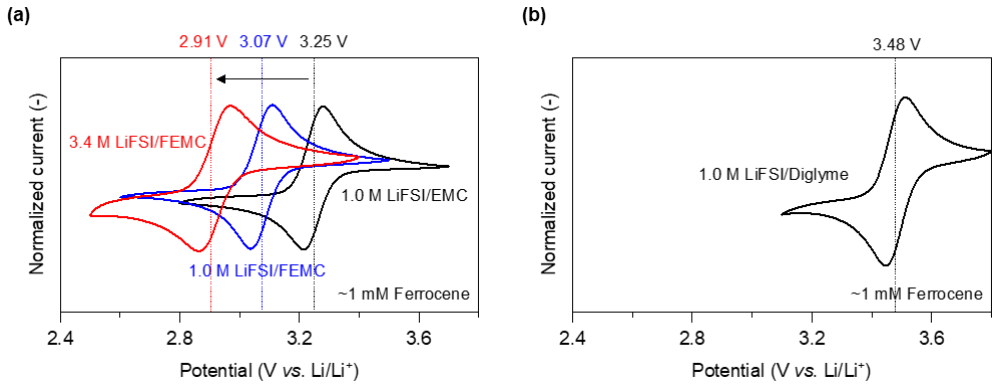

Supplementary Figure 5. (a–b) Cyclic voltammograms of ferrocene (Fc) in various electrolytes. The redox potential of Li/Li^+ (V *vs.* Fc/Fc^+) is gradually upshifted with a change in the solution structure of the electrolyte from solvent-separated ion pairs to ion-pair aggregates (Fig. 2).

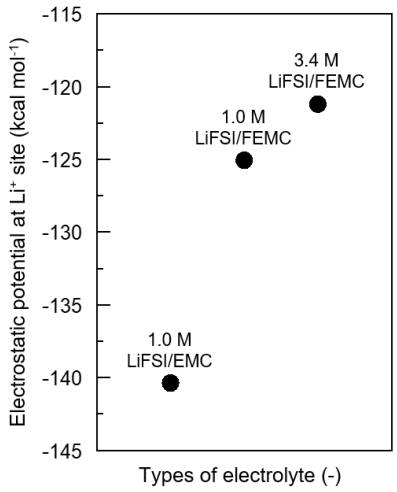

Supplementary Figure 6. Calculated stabilities of Li^+ (electrostatic potentials at the Li^+ sites) in the given electrolytes. Li^+ is electrostatically destabilized in dense ion-pair aggregates in 3.4 M LiFSI/FEMC, which contributes to upward shifts in the redox potentials of Li/Li^+ and the related electrode potential.

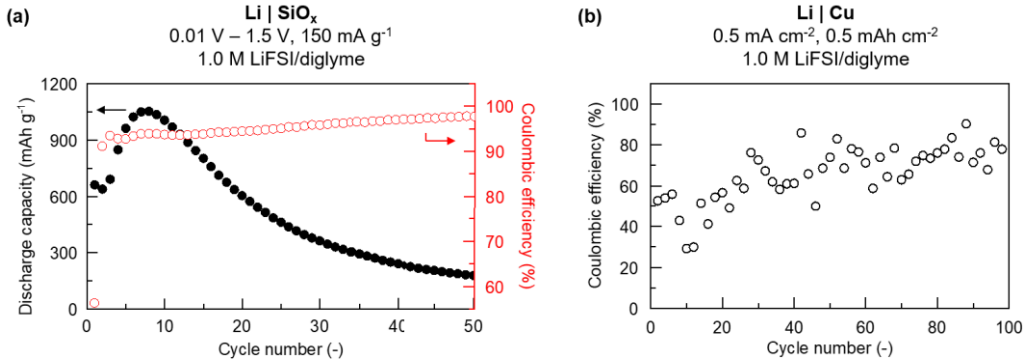

Supplementary Figure 7. (a) Discharge capacity and Coulombic efficiency of an Li|SiO_x half-cell with a 1.0 M LiFSI/diglyme electrolyte. The loading level of the SiO_x electrode was 1 mg cm^{-2}. (b) Coulombic efficiency of Li plating/stripping on Cu foil in 1.0 M LiFSI/diglyme. A combined separator, composed of PP and glass fiber separators, was used.

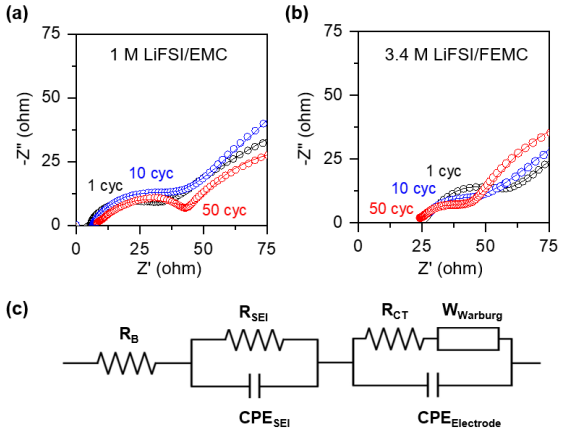

Supplementary Figure 8. Nyquist plots of SiO_x electrodes cycled in (a) 1.0 M LiFSI/EMC and (b) 3.4 M LiFSI/FEMC. The interfacial resistance of the electrode increases negligibly after 50 cycles in 3.4 M LiFSI/FEMC, suggesting that the SiO_x surface (including the SEI) is effectively protected during lithiation/delithiation (expansion/shrinkage). (c) Equivalent circuit model employed to fit the Nyquist plots.

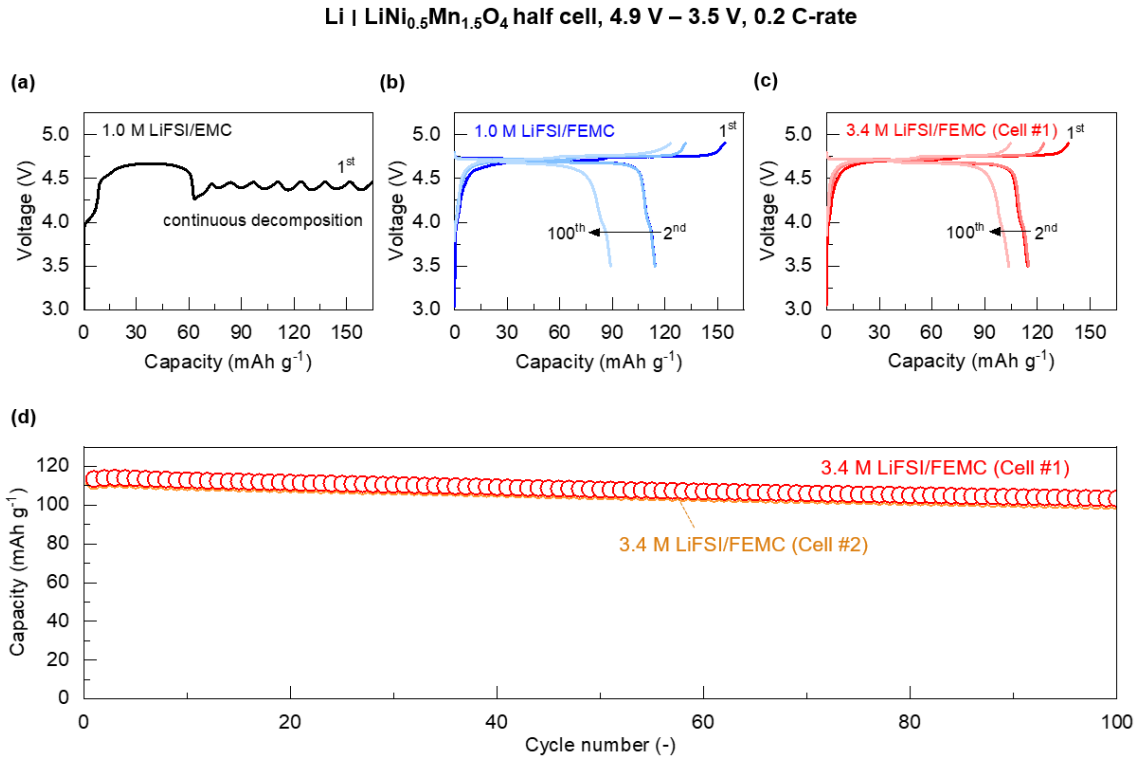

Supplementary Figure 9. Charge and discharge curves of Li|$LiNi_{0.5}Mn_{1.5}O_4$ half-cells with (a) 1.0 M LiFSI/EMC, (b) 1.0 M LiFSI/FEMC, and (c) 3.4 M LiFSI/FEMC electrolytes. (d) Reproducibility of the cell with 3.4 M LiFSI/FEMC. The loading levels of the $LiNi_{0.5}Mn_{1.5}O_4$ electrodes were 3 mg cm^{-2}. Combined separators, composed of cellulose and glass fiber separators, were used. The C-rate was calculated based on the theoretical capacity of $LiNi_{0.5}Mn_{1.5}O_4$ (147 mAh g^{-1}).

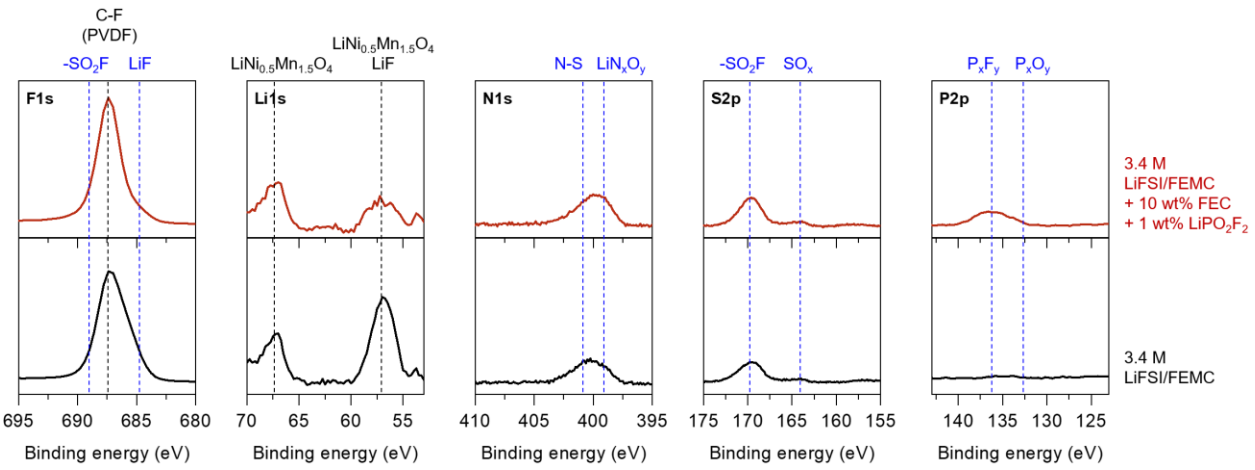

Supplementary Figure 10. X-ray photoelectron spectra of the $LiNi_{0.5}Mn_{1.5}O_4$ electrodes cycled in various electrolytes. The electrodes comprised 80, 10, and 10 wt.% $LiNi_{0.5}Mn_{1.5}O_4$, amorphous carbon black, and PVDF binder, respectively. They were cycled ten times between 4.9 and 3.5 V. The $LiNi_{0.5}Mn_{1.5}O_4$-derived signals (Li1s) are detected, indicating that their surfaces are partially covered with porous and/or thin passivation films in the given electrolytes. The electrolyte additives (FEC and $LiPO_2F_2$) were introduced to increase the wettability and scavenge HF, thus ensuring the extremely stable long-term cycling of a full cell (Supplementary Figs. 16 and 17).

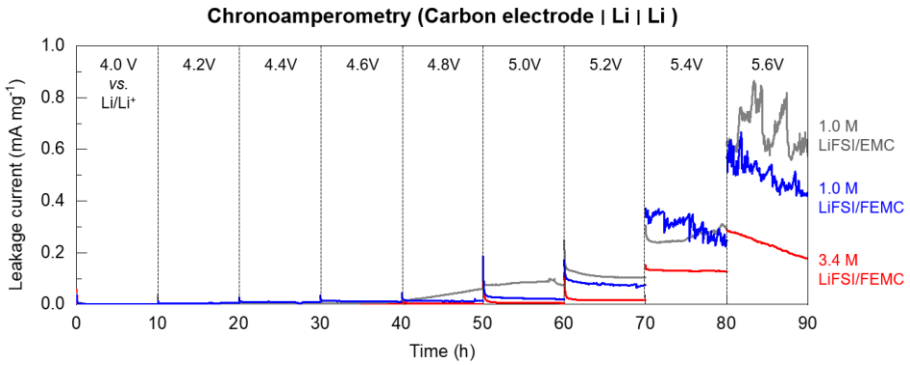

Supplementary Figure 11. Electrochemical floating tests of conductive carbon additive/polyvinylidene fluoride (PVDF) binder (1/1, w/w) electrodes coated onto Al current collectors at loading levels of 1.7–1.8 mg cm^{-2}. The 3.4 M LiFSI/FEMC electrolyte displays a higher oxidative stability than those of 1.0 M LiFSI/EMC and 1.0 M LiFSI/FEMC.

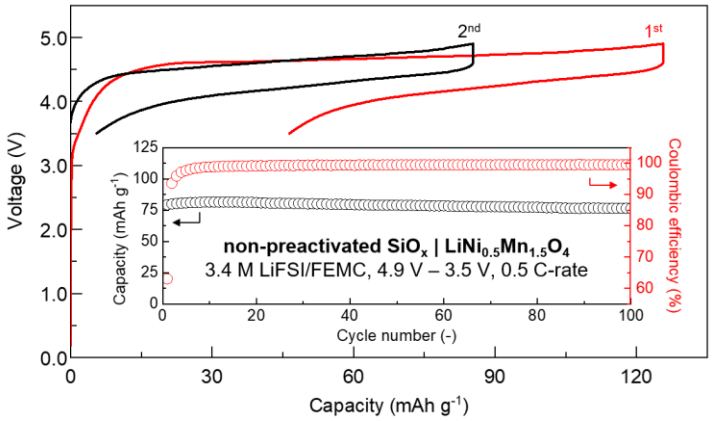

Supplementary Figure 12. Charge and discharge curves of a non-preactivated full SiO_x|$LiNi_{0.5}Mn_{1.5}O_4$ cell with 3.4 M LiFSI/FEMC. The loading level of the $LiNi_{0.5}Mn_{1.5}O_4$ electrode was 3.5 mg cm^{-2}, the N/P ratio was controlled at 1.3, and a glass fiber separator was used. The capacity was calculated based on the weight of the cathode active materials. The Coulombic efficiency and initial discharge capacity of the cell are 63 % and 79 mAh g^{-1}, respectively, indicating that the activation of SiO_x requires a large amount of the Li source.

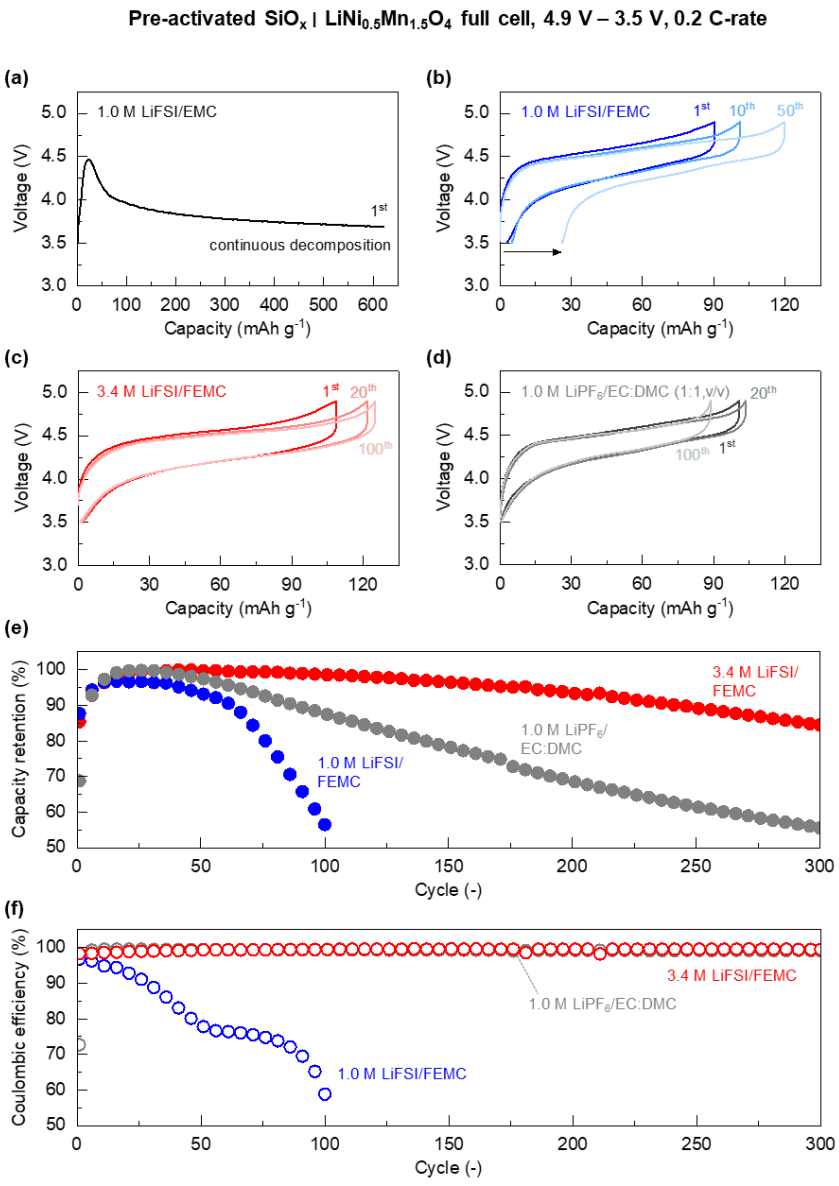

Supplementary Figure 13. Charge and discharge curves of pre-activated full SiO_x|$LiNi_{0.5}Mn_{1.5}O_4$ cells with upper cut-off voltages of 4.9 V at low constant C-rates of 0.2C in (a) 1.0 M LiFSI/EMC, (b) 1.0 M LiFSI/FEMC, (c) 3.4 M LiFSI/FEMC, and (d) 1.0 M $LiPF_6$/ethylene carbonate (EC):dimethyl carbonate (DMC) (1:1, v/v) electrolytes. (e–f) Cycling stabilities and Coulombic efficiencies of the cells with the given electrolytes. Every fifth point is plotted, and the loading levels of the $LiNi_{0.5}Mn_{1.5}O_4$ electrodes were ~5 mg cm^{-2}. The N/P ratios were controlled at ~1.5, and glass fiber separators were used. The capacity was calculated based on the weight of the cathode active materials.

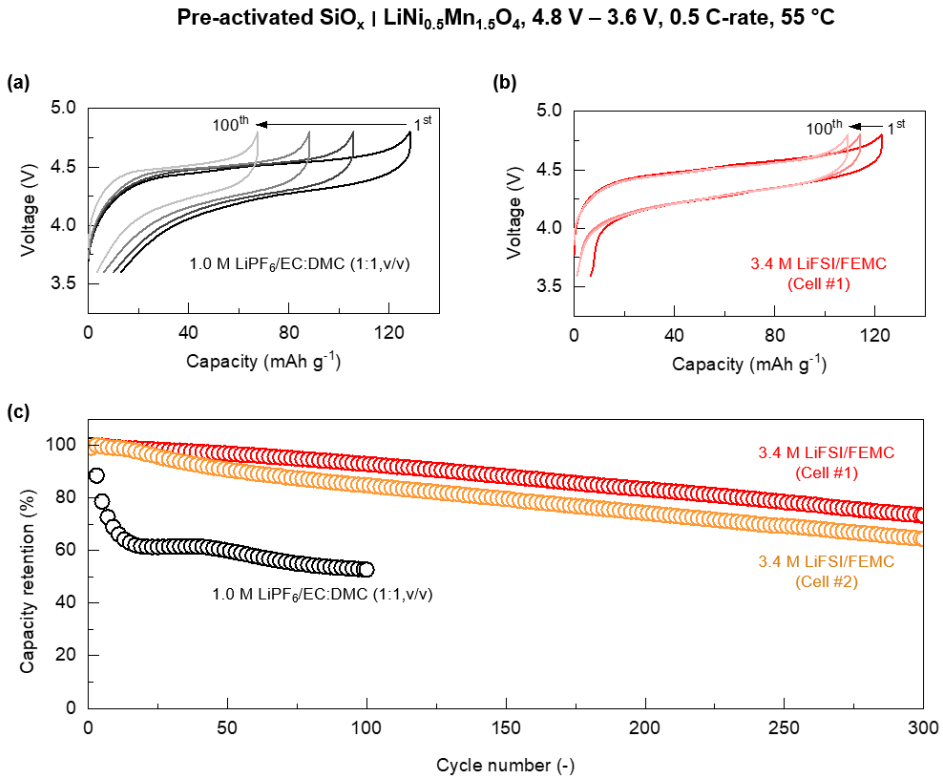

Supplementary Figure 14. Charge and discharge curves of pre-activated full SiO_x|$LiNi_{0.5}Mn_{1.5}O_4$ cells with upper cut-off voltages of 4.8 V at low constant C-rates of 0.5C in (a) 1.0 M $LiPF_6$/EC:DMC (1:1, v/v) and (b) 3.4 M LiFSI/FEMC at 55 ºC. (c) Discharge capacity retentions of the full cells at 55 ºC in the given electrolytes as functions of the cycle number. The reproducibility was verified using two cells, and the loading levels of the $LiNi_{0.5}Mn_{1.5}O_4$ electrodes were ~3 mg cm^{-2}. The N/P ratios were controlled at ~1.8, and glass fiber separators was used. The capacity was calculated based on the weight of the cathode active materials. To stabilize the SEIs, the full cells were cycled 10 times at 25 ºC at C-rates of 0.2C before conducting the high-temperature study. Every second point is plotted.

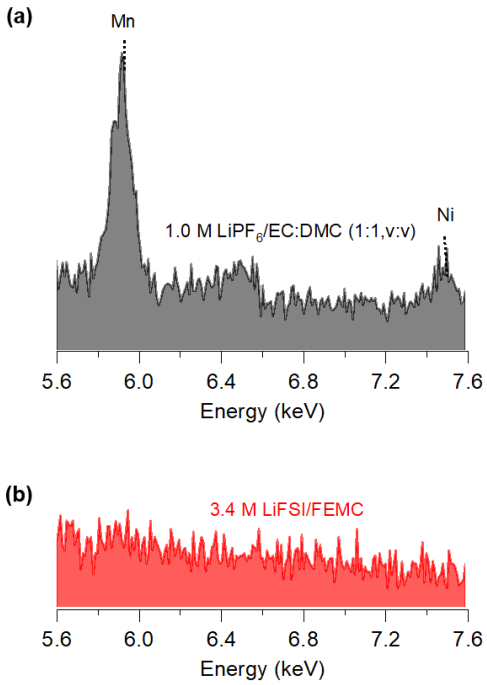

Supplementary Figure 15. Energy-dispersive X-ray (EDX) spectra of the SiO_x electrodes in the pre-activated full SiO_x|$LiNi_{0.5}Mn_{1.5}O_4$ cells cycled at 55 ºC with the different electrolytes. The dissolution of transition metals from the cathode materials and their deposition on the anode severely deteriorate battery performance. Based on the results of EDX spectroscopy, higher amounts of deposited Mn and Ni are detected using 1.0 M $LiPF_6$/EC:DMC (1:1, v/v) than those detected using 3.4 M LiFSI/FEMC. The suppressed transition metal dissolution in 3.4 M LiFSI/FEMC may be explained as follows. Firstly, the generation of acidic HF, which damages the surfaces of cathode materials, is alleviated due to the prevention of hydrolysis of FSI^-, with its high chemical and thermal stabilities compared to those of PF_6^-. Additionally, the H- and F-abstraction reactions of the FEMC solvent and FSI^- are retarded, based on the high oxidative stability of the fluorinated electrolyte with an ion pair-dominated solution structure. In addition, although the dissolution of transition metals occurs at the damaged surface, their diffusion into the bulk electrolyte is unfavorable because of the poor dissolution and weak solvating properties of the electrolyte.

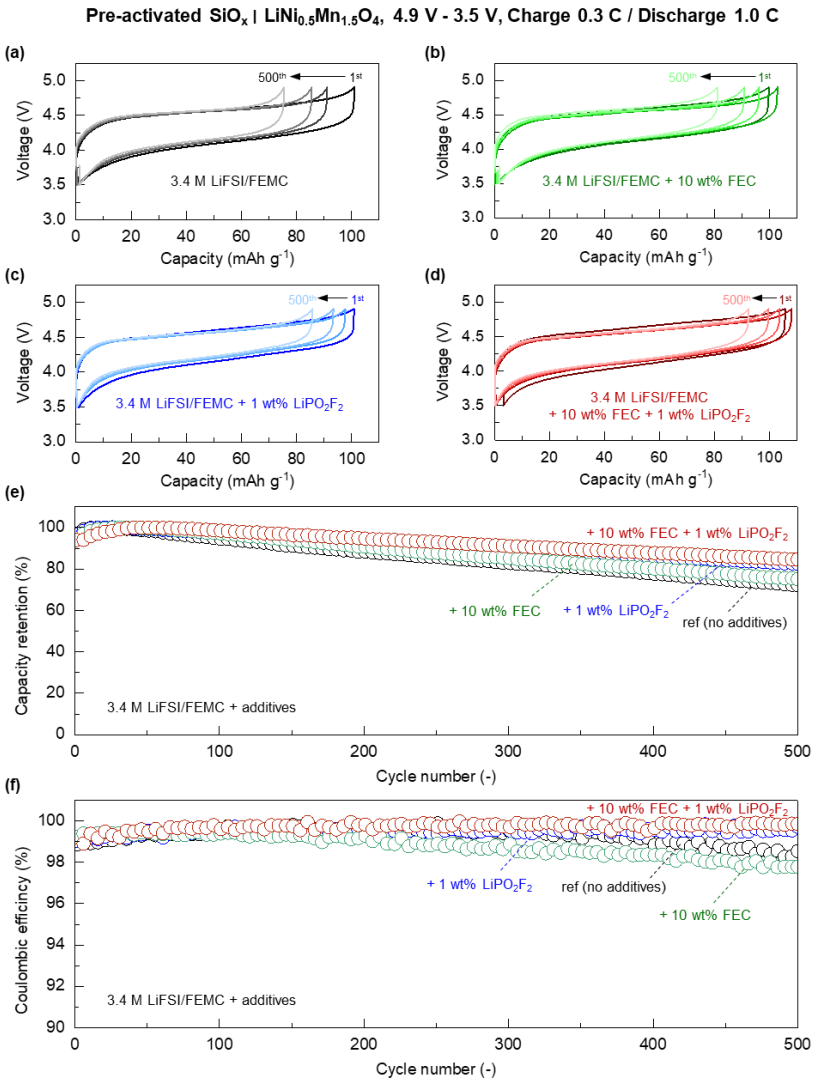

Supplementary Figure 16. (a–d) Charge and discharge curves, (e) discharge capacity retentions, and (f) Coulombic efficiencies of the pre-activated full SiO_x|$LiNi_{0.5}Mn_{1.5}O_4$ coin-type cells under various conditions. Every fifth point is plotted. The capacity was calculated based on the weight of the cathode active materials. The details of cell information are demonstrated in Table S3.

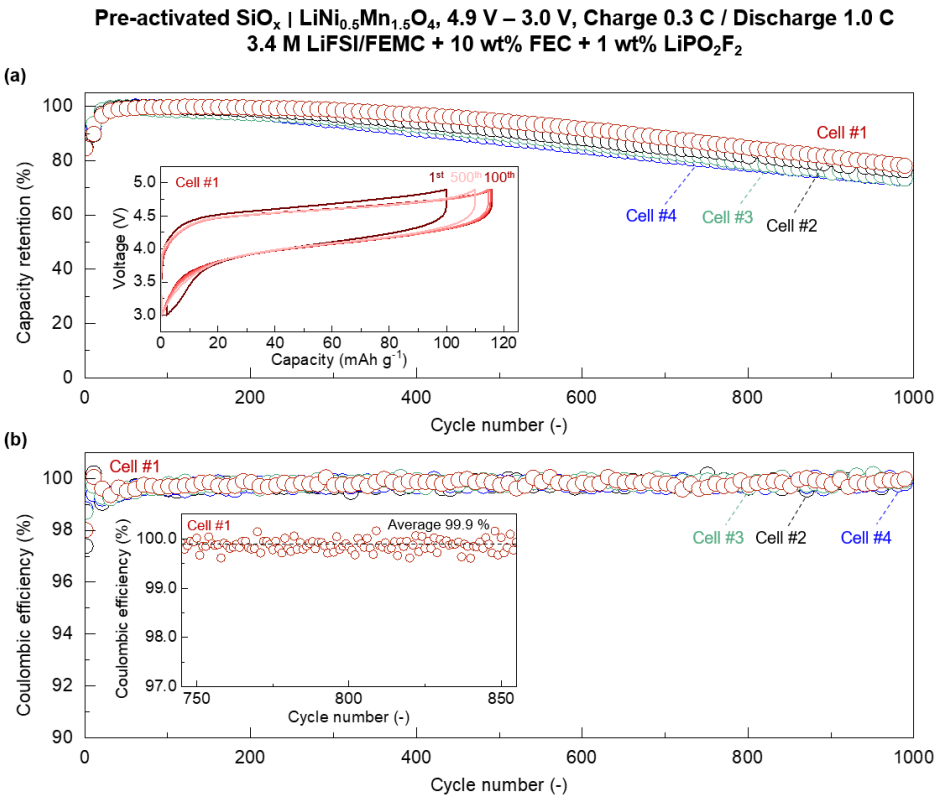

Supplementary Figure 17. Reproducibility of the pre-activated full SiO_x|$LiNi_{0.5}Mn_{1.5}O_4$ coin-type cell with the 3.4 M LiFSI/FEMC + 10 wt.% FEC + 1 wt.% $LiPO_2F_2$ electrolyte. Every tenth point is plotted. The capacity was calculated based on the weight of the cathode active materials. The details of cell information are demonstrated in Table S3.

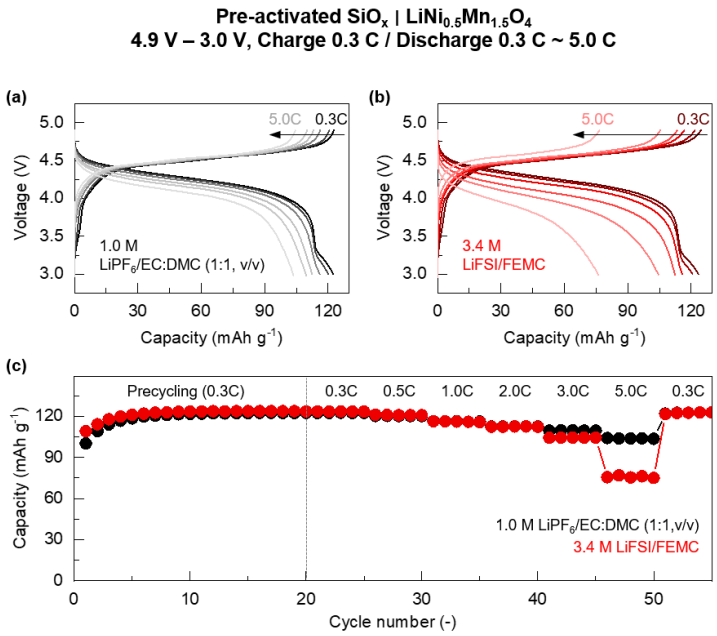

Supplementary Figure 18. Rate performances of the pre-activated full SiO_x|$LiNi_{0.5}Mn_{1.5}O_4$ cells in 3.4 M LiFSI/FEMC and standard 1.0 M $LiPF_6$/EC:DMC (1:1, v/v) electrolytes. The loading levels of the cathodes were 11 mg cm^{-2}, and the N/P ratios were 1.2~1.3. The capacity was calculated based on the weight of the cathode active materials. Following the general trend of concentrated (ion-pair-based) electrolytes, the ion conductivity of 3.4 M LiFSI/FEMC (1.2 mS cm^{-1}) is lower than that of standard 1.0 M $LiPF_6$/EC:DMC (10 mS cm^{-1}). This makes the rate performance competitive at <3C but a bit inferior at >5C.

Supplementary References

1. He, D. *et al.* Collaborative design of hollow nanocubes, in situ cross-linked binder, and amorphous Void@SiO_x@C as a three-pronged strategy for ultrastable lithium storage. *Small* **16**, (2020).

2. Kim, H. J. *et al.* Controlled prelithiation of silicon monoxide for high performance lithium-ion rechargeable full cells. *Nano Lett.* **16**, 282–288 (2016).

3. Fang, S. *et al.* Highly graphitized carbon coating on SiO with a π-π stacking precursor polymer for high performance lithium-ion batteries. *Polymers* **8**, (2018).

4. Meng, Q. *et al.* High-performance lithiated SiO_x anode obtained by a controllable and efficient prelithiation strategy. *ACS Appl. Mater. Interfaces* **11**, 32062–32068 (2019).

5. Wu, H. *et al.* Recycling silicon-based industrial waste as sustainable sources of Si/SiO_2 composites for high-performance Li-ion battery anodes. *J. Power Sources* **449**, (2020).

6. Huang, Q. *et al.* Supremely elastic gel polymer electrolyte enables a reliable electrode structure for silicon-based anodes. *Nat. Commun.* **10**, (2019).

7. Liu, Z. *et al.* Monodisperse and homogeneous SiO_x/C microspheres: A promising high-capacity and durable anode material for lithium-ion batteries. *Energy Stor. Mater.* **13**, 112–118 (2018).

8. Zhao, H. *et al.* Toward practical application of functional conductive polymer binder for a high-energy lithium-ion battery design. *Nano Lett.* **14**, 6704–6710 (2014).

9. Liang, J. *et al.* A deep reduction and partial oxidation strategy for fabrication of mesoporous Si anode for lithium ion batteries. *ACS Nano* **10**, 2295–2304 (2016).

10. Zhang, Y. *et al.* Mechanical constraining double-shell protected Si-based anode material for lithium-ion batteries with long-term cycling stability. *J. Alloys Compd.* **846**, (2020).

11. Yan, M. Y. *et al.* Enabling SiO_x/C anode with high initial coulombic efficiency through a chemical pre-lithiation strategy for high-energy-density lithium-ion batteries. *ACS Appl. Mater. Interfaces* **12**, 27202–27209 (2020).

12. Cho, Y. *et al.* A pyrene-poly(acrylic acid)-polyrotaxane supramolecular binder network for high-performance silicon negative electrodes. *Adv. Mater.* **31**, (2019).

13. Liu, D., Jiang, Z., Zhang, W., Ma, J. & Xie, J. Micron-sized SiO_x/N-doped carbon composite spheres fabricated with biomass chitosan for high-performance lithium-ion battery anodes. *RSC Adv.* **10**, 38524–38531 (2020).

14. He, W. *et al.* Efficient synthesis of N-doped SiO_x/C composite based on the defect-enriched graphite flake for lithium-ion battery. *ACS Appl. Energy Mater.* **3**, 4394–4402 (2020).

15. Hu, G. *et al.* Surface oxidation layer-mediated conformal carbon coating on si nanoparticles for enhanced lithium storage. *ACS Appl. Mater. Interfaces* **13**, 3991–3998 (2021).

16. Huang, B., Huang, T., Wan, L. & Yu, A. P Pre-lithiating SiO anodes for lithium-ion batteries by a simple, effective, and controllable strategy using stabilized lithium metal powder. *ACS Sustain. Chem. Eng.* **9**, 648–657 (2021).

17. Huang, B., Chu, B., Huang, T. & Yu, A. Nitrogen-doped carbon-coating disproportionated SiO materials as long cycling stable anode for lithium ion batteries. *Molecules* **26**, (2021).

18. Zhang, K. *et al.* SiO_x embedded in N-doped carbon nanoslices: A scalable synthesis of high-performance anode material for lithium-ion batteries. *Carbon* **178**, 202–210 (2021).

19. Sun, Q., Li, J., Hao, C. & Ci, L. Focusing on the subsequent Coulombic efficiencies of SiO_x: Initial high-temperature charge after over-capacity prelithiation for high-efficiency SiO_x-based full-cell battery. *ACS Appl. Mater. Interfaces* **14**, 14284–14292 (2022).

20. Kim, J. W., Seong, M. J., Park, D. W., Jeong, G. & Yim, T. Anti-corrosive and surface-stabilizing functional electrolyte containing LiFSI and $LiPO_2F_2$ for SiO_x/NCM811-based batteries. *Corros. Sci.* **198**, (2022).

21. Werner, D., Paarmann, S. & Wetzel, T. Calendar aging of Li-ion cells—Experimental investigation and empirical correlation. *Batteries* **7**, 28 (2021).

22. Sun, S. *et al.* Accelerated aging and degradation mechanism of $LiFePO_4$/graphite batteries cycled at high discharge rates. *RSC Adv.* **8**, 25695–25703 (2018).

23. Gao, Z. *et al.* The dilemma of C-rate and cycle life for lithium-ion batteries under low temperature fast charging. *Batteries* **8**, 234 (2022).

24. Murray, V., Hall, D. S. & Dahn, J. R. A guide to full coin cell making for academic researchers. *J. Electrochem. Soc.* **166**, A329–A333 (2019).

25. Cui, Y. *et al.* Multi-stress factor model for cycle lifetime prediction of lithium ion batteries with shallow-depth discharge. *J. Power Sources* **279**, 123–132 (2015).